Ergodicity breaking in stronium calcium titanate

2001 J. Phys.: Condens. Matter 13 2615

(http://iopscience.iop.org/0953-8984/13/11/317)

INSTITUTE OF PHYSICS PUBLISHING JOURNAL OF PHYSICS: CONDENSED MATTER

J. Phys.: Condens. Matter **13** (2001) 2615–2626 www.iop.org/Journals/cm PII: S0953-8984(01)17759-3

Ergodicity breaking in stronium calcium titanate

M T Lacerda-Arôso[1], J L Ribeiro[1], M R Chaves[2], B G Almeida[1] and A Almeida[2]

[1] Departamento de Física, Universidade do Minho, 4710-057 Braga, Portugal
[2] Departamento de Física, IMAT (núcleo IFIMUP), Faculdade de Ciências da Universidade do Porto, Rua do Campo Alegre 687, 4169-007 Porto, Portugal

E-mail: jlr@fisica.uminho.pt

Received 14 October 2000, in final form 22 December 2000

Abstract

This work reports experimental results obtained from series of measurements of pyroelectric currents in samples of strontium calcium titanate (SCT) corresponding to contents of Ca of $x = 0.002$, $x = 0.005$ and $x = 0.011$. Sequences of zero field cooling (zfc), field heating (fh), field cooling (fc) and zero field heating (zfh) runs, under different applied electric fields, allowed the observation of the temperature and field dependence of the electric polarization under different initial conditions. The results show the existence of a weak non-ergodic regime in the compositions $x = 0.005$ and $x = 0.011$ and allow the tracing of the corresponding Almeida–Thouless line in the T–E diagram. For the three compositions investigated, a small zero field polarization is detected and interpreted as due to defect induced internal fields.

1. Introduction

Strontium titanate (ST: $SrTiO_3$), like $KTaO_3$, is a well known example of a quantum paraelectric [1]. At room temperature, this material has a perovskite structure (symmetry O_h) and, at $T_{c1} = 105$ K, the softening of a lattice mode related to the anti-symmetric rotation of the oxygen octahedra around the cubic [001] axis induces an anti-ferrodistortive phase (symmetry D_{4h}) [2]. At temperatures $T < T_{c1}$, the progressive softening of a long wavelength polar transverse optical mode gives rise to a strong increase of the static dielectric constant [3]. The onset of a long range ferroelectric order is however suppressed by quantum fluctuations, and the increase of the dielectric constant saturates below $T = 4$ K [4].

The inclusion of lattice impurities in a quantum paraelectric gives rise to interesting phenomena which have been studied extensively in systems like $K_{1-x}Li_xTaO_3$ (KTL) or $KTa_{1-x}Nb_xO_3$ (KTN) as well as in $Sr_{1-x}Ca_xTiO_3$ (SCT) [5–9]. The inclusion of calcium in ST induces local dipoles, which may be caused either by local deformation of the lattice, when Ca replaces Sr (non-central or A-site impurity), or by the Ca^{2+}–V_o (V_o: oxygen vacancy) centres that are formed when Ca^{2+} replaces Ti^{4+} at the unit cell centre (central or B-site impurity).

0953-8984/01/112615+12$30.00

Unlike the case of alkali halide dielectrics with extrinsic dipoles, where the fluctuation of local dipolar fields prevents the onset of long range order, the increase of the concentration of impurities in a system like SCT may originate ferroelectricity [5]. Such an impurity induced phase transition is a consequence of the high polarizability of the host medium: the lattice not only becomes polarized in the vicinity of an extrinsic dipole (thus giving rise to extended polar regions) but also modifies the effective interaction between extrinsic dipoles, which may turn out to be predominantly ferroelectric and more complicated than the usual dipole–dipole interaction [5]. For a high enough concentration of impurities, the configurational fluctuations of the local fields can decline as the temperature is lowered, giving rise to a long range ferroelectric order.

Hence, the ferroelectric ordering in SCT would result from the thermal growth of the polar clusters surrounding the Ca^{2+} impurities, as the temperature decreases. In fact, this percolative process is expected to produce an intermediate superparaelectric state of random cluster-like polar nanoregions, which gives rise to the high non-linear dielectric response found in SCT [10, 11].

However, as the strength of the dipolar interaction between clusters and the intensity and orientation of the local fields induced by the lattice are random variables, each cluster can be submitted to conflicting interactions. Under certain conditions, disorder can prevail over long-range order and a polar glass phase may be stabilized. In this case, the phase space at low temperatures may be represented as an irregular landscape made of valleys (metastable states) and mountains (barriers) between them. If the barriers are high enough, the system may be trapped into a particular valley and its physical properties may depend on the local sub-space in which it is confined. The system becomes non-ergodic.

The effects of disorder and the possibility of ergodicity breaking are not usually taken into account in most of the models adopted to describe the dielectric behaviour of SCT, which range from the Barrett formula [12] (or its heuristic modification based on the idea of the so-called quantum temperature scale [13]) to spin models such as the transverse Ising model [14].

Recently, a modified Sherrington–Kirkpatrick model [15] was tentatively adopted to describe the competition between ferro interactions, quantum fluctuations and disorder in systems like SCT [16, 17]. At low temperatures, this model generates a phase diagram that includes the stabilization of para, ferro or glassy phases, depending on the relative strength of the long range ferroelectric interaction (J_0), the tunnelling energy (A) and the random disorder (J_1). Similar to magnetic spin glasses, the system is expected to become non-ergodic at low temperatures for certain values of these parameters.

Alberici *et al* [18] reported an experimental study of the time dependence of the complex dielectric constant along the [100] pseudo-cubic axis of the SCT crystal with a Ca content of $x = 0.005$. This time dependence was measured at a constant temperature of 4.2 K, using frequencies ranging from 1 kHz to 1 MHz, after different thermal histories. This study showed not only the existence of aging but also that the asymptotic values of both real and imaginary components of the dielectric constant at large times were dependent on the thermal history of the sample. This observation, by indicating that the equilibrium state is dependent on the initial conditions, demonstrates the existence of a non-ergodic regime at low temperatures in this compound.

This work reports additional results obtained in series of measurements of dielectric constant and pyroelectric currents in samples of SCT corresponding to nominal contents of Ca of $x' = 0.002$, $x' = 0.01$ and $x' = 0.025$. Using the relation between the location of the dielectric peak at T^{**} (see figure 1) with the calcium content x in the crystal reported in [6] ($T_{max} \approx 298\sqrt{x - 0.0018}$ K), we ascribe the effective compositions of $x = 0.002$, $x = 0.005$ and $x = 0.011$ to the samples with nominal compositions of $x' = 0.002$, $x' = 0.01$

and $x' = 0.025$, respectively. The measurement of pyroelectric currents in sequences of zero field cooling (zfc) field heating (fh), field cooling (fc) and zero field heating (zfh) runs, under different applied electric fields, allowed the observation of the temperature and field dependence of the electric polarization under different initial conditions. The results indicate the existence of a weak non-ergodic regime (in the sense of Bouchaud [19]) for the compositions $x = 0.005$ and $x = 0.011$, and allow the tracing of the corresponding Almeida–Thouless line [20] in the T–E diagram.

2. Experiment

The samples were cut from crystals with effective compositions of $x = 0.002$, $x = 0.005$ and $x = 0.011$ as parallel plates perpendicular to the [100] pseudo-cubic axis. The typical dimensions of the samples were $6 \times 1 \times 0.3$ mm^3. This geometry favours the onset at T_{c1} of an oriented state with the tetragonal c-axis parallel to the long edge of the sample [21]. The major faces were electroded by gold vapour deposition. The samples, in a cryogenic environment, were connected either to the output port of an HP 4192A impedance analyser or to a Keithley 617 electrometer for dielectric or pyroelectric measurements, respectively.

The dielectric constant data was collected at 1.5 kHz with a constant ac voltage of 0.2 V. For the measured samples, this voltage corresponds to field amplitudes in the range 0.25–0.8 kV m^{-1}. The heating and cooling rates were of the order of 0.5 K min^{-1}. The pyroelectric currents were measured by heating or cooling the samples at a rate of the order of 1 K min^{-1}, in sequences of thermal cycles: the samples were cooled down without any bias field (zero-field cooling), heated up and cooled down under a certain bias (field heating and field cooling) and, finally, heated up at zero bias field (zero-field heating). In each heating run, the samples were heated over 120 K, thus crossing the tetragonal–cubic anti-distortive phase transition. At this crossing, no special care (other than the choice of the particular geometry of the samples) was taken to minimize the formation of elastic domains. The electric polarization was calculated by time integration of the pyroelectric current.

3. Results and discussion

Figures 1(a)–(c) display the real (ε') and the imaginary (ε'') parts of the dielectric constant, as function of temperature, measured in samples corresponding to the three compositions under study. For the composition $x = 0.002$, ε' and ε'' increase as the temperature decreases and exhibit maxima at about $T^* = 12$ K. For $x = 0.005$ (figure 1(b)), ε' shows a maximum at $T^{**} = 17$ K, while ε'' displays a shoulder at about T^{**} and a maximum at $T^* = 12$ K. Further increase of the calcium content ($x = 0.01$, figure 1(c)) shifts T^{**} towards higher temperatures ($T^{**} = 27$ K) and increases the intensity of the corresponding anomaly in ε'. T^* is also shifted to values of the order of 16 K.

These data are essentially in agreement with previous reported results [6, 22]. The dielectric anomaly observed near T^* has also been detected in the dielectric loss ε'' of nominally pure ST and in KTN, although with smaller intensities. In the case of ST, this anomaly has been related to a possible transition to a so-called quantum-coherent state [23], proposed by Müller *et al* [24]. Its origin has also been related to solitonic excitations between tilted domains [25] or to polaronic excitations [26]. Similar anomalies have been also detected in pure and Bi doped ST ceramics [27], in which the temperature of the dielectric loss peak is independent of the dopant concentration. This observation suggests that some mechanisms intrinsic to the host lattice might be involved, but their nature remains unclear. Recently, these anomalies were also attributed to the very low background of unavoidable impurities [28].

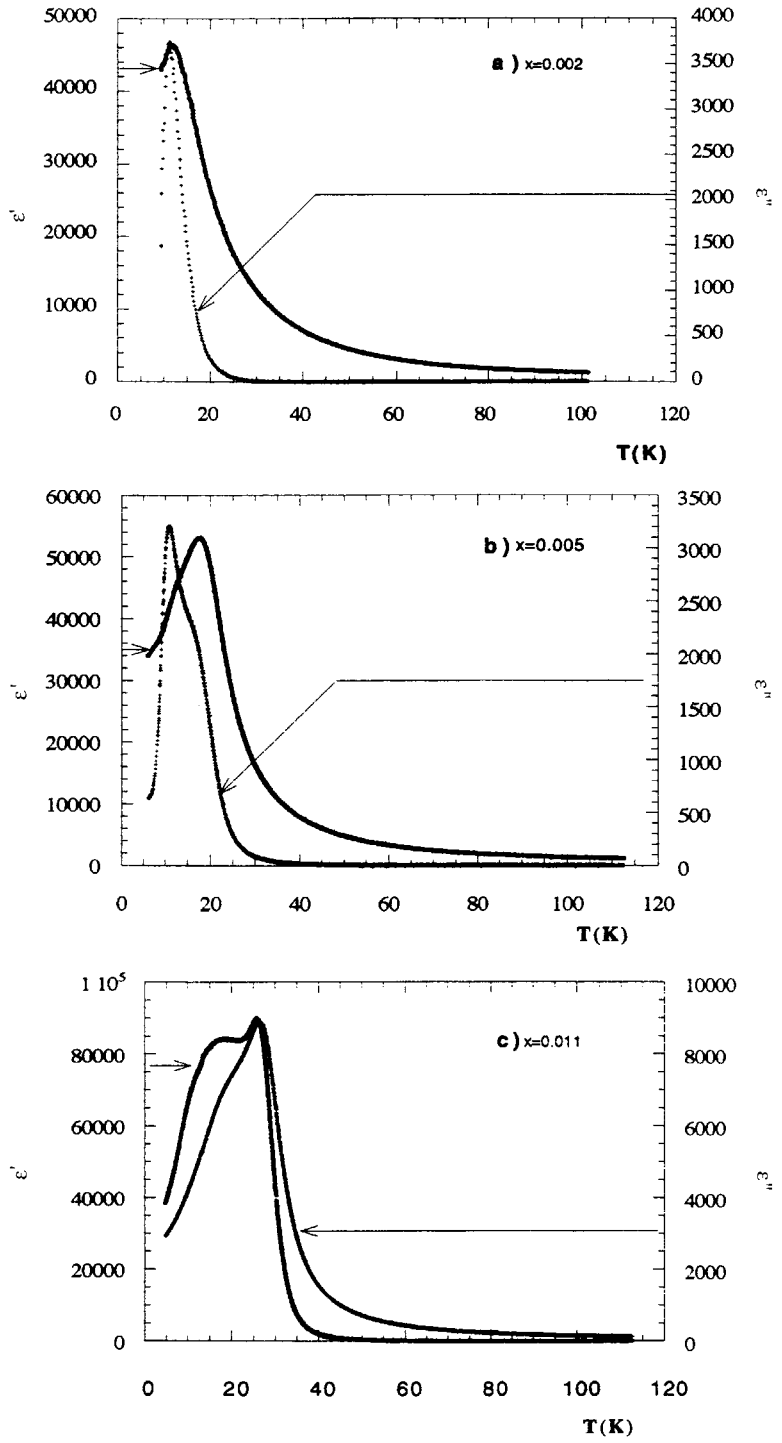

Figure 1. Real and imaginary parts of the relative dielectric constant $\varepsilon = \varepsilon' + \mathrm{i}\varepsilon''$ of $SrTiO_3$:$_x$Ca for calcium concentrations corresponding to (a) $x = 0.002$, (b) $x = 0.005$ and (c) $x = 0.011$. Data taken with an HP 4192A LCR-meter under the best measuring fields herein: 0.1 or 0.2 V_{ac} and 1.5 kHz.

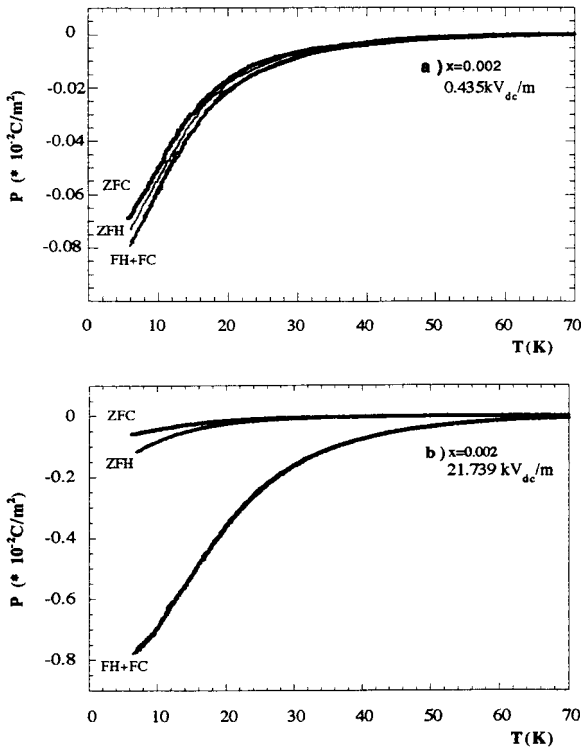

Figure 2. ZFC–FH–FC–ZFH polarization cycles measured by the pyroelectric effect in the ergodic $x = 0.2\%$ composition crystal using two far apart values of dc field: (a) $E = 0.435$ kV m^{-1} and (b) $E = 21.739$ kV m^{-1}.

On the other hand, the location and intensity of the dielectric peak at T^{**} clearly depend on the Ca content. Its origin has been related to the onset of a Ca induced displacive transition to a ferroelectric phase [6]. Similar anomalies were observed in Bi doped ST ceramics above a certain threshold concentration of impurities [29].

Figures 2–4 show examples of the temperature dependence of the electric polarization along sequences of zero field cooling, field heating, field cooling and zero field heating runs, measured under different fields in samples corresponding to $x = 0.002$ (figure 2), $x = 0.005$ (figure 3) and $x = 0.011$ (figure 4). Note that, for all compositions investigated, small polarizations of the order of 10^{-4} C m^{-2} are observed in the zfc runs. The nature of these small zfc polarizations will be discussed at the end of this section.

As can be seen in figure 2, for $x = 0.002$ and in the range of fields scanned, the modulus of the electric polarization increases monotonically with the bias field. Within the experimental resolution, the fh and fc polarization curves coincide. This indicates that, under a bias field, the dielectric response of the system depends only on temperature and is independent of the previous thermal history. In other words, under a bias field, the system responds ergodically. However, the zfh depolarization obtained after a field cooling run perceives a slow and thermally activated relaxation process and suggests that a partial dipolar freezing occurs at zero field.

The increase of the Ca concentration strongly alters this behaviour (figures 3 ($x = 0.005$) and 4 ($x = 0.011$)). A first remark concerns the fact that the zfc polarizations are depicted as negative. This means that the electric fields in the subsequent runs were applied in a sense opposite to the initial polarization and induce reversed (positive) polarizations. As can be seen,

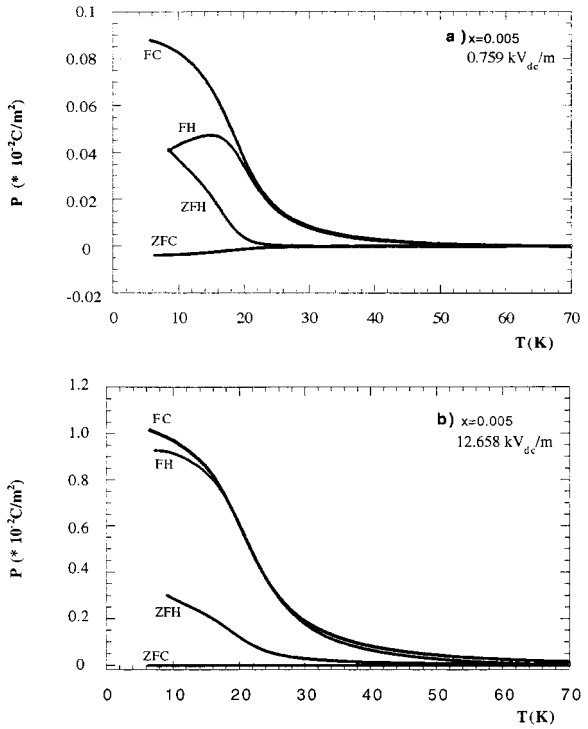

Figure 3. Examples of $P(T)$ curves measured in ZFC–FH–FC–ZFH cycles for $x = 0.005$: (a) $E = 0.759\ \mathrm{kV\ m^{-1}}$, (b) $E = 12.658\ \mathrm{kV\ m^{-1}}$. Under different dc fields, a progressive decrease of the Almeida–Thouless temperature is evidenced by the splitting of the FH–FC polarization curves. A permanent residual polarization (negative with respect to the applied bias field) is observed in the ZFC runs.

for these two compositions, the low temperature $P(T)$ curves depend on the thermal history. As in spin glasses, this indicates an effective non-ergodic response at low temperatures. As the temperature increases, the fh and the fc $P(T)$ curves merge together at a field dependent temperature T_{A-T} and coincide for higher temperatures. This field dependent temperature marks therefore the border between an ergodic and an effective non-ergodic region in the (T, E) plane.

Figure 5 displays the $E(T_{A-T})$ lines for the $x = 0.005$ (squares) and $x = 0.011$ (circles) compositions, estimated from different thermal cycles at different bias fields. Qualitatively, these curves are similar to those observed in spin glasses, which were discussed by Almeida and Thouless on the basis on the mean-field Sherrington–Kirkpatrick (S–K) model. This line, the Almeida–Thouless line, would correspond to the border between a high temperature region where the replica trick (upon which the S–K is based) is valid, and a lower temperature region where it fails. The failure of the replica trick, being linked to the breaking of self-similarity in phase space, would correspond to the onset of a non-ergodic regime.

It is tempting to explore a little more the analogy with spin glasses. As shown by Almeida and Thouless [20], the equation of the A–T line $T(H)$ for a spin glass in a S–K approximation can be written as

$$\left[\frac{T(H)}{T(0)}\right]^2 = 1 - 2q + r \tag{1}$$

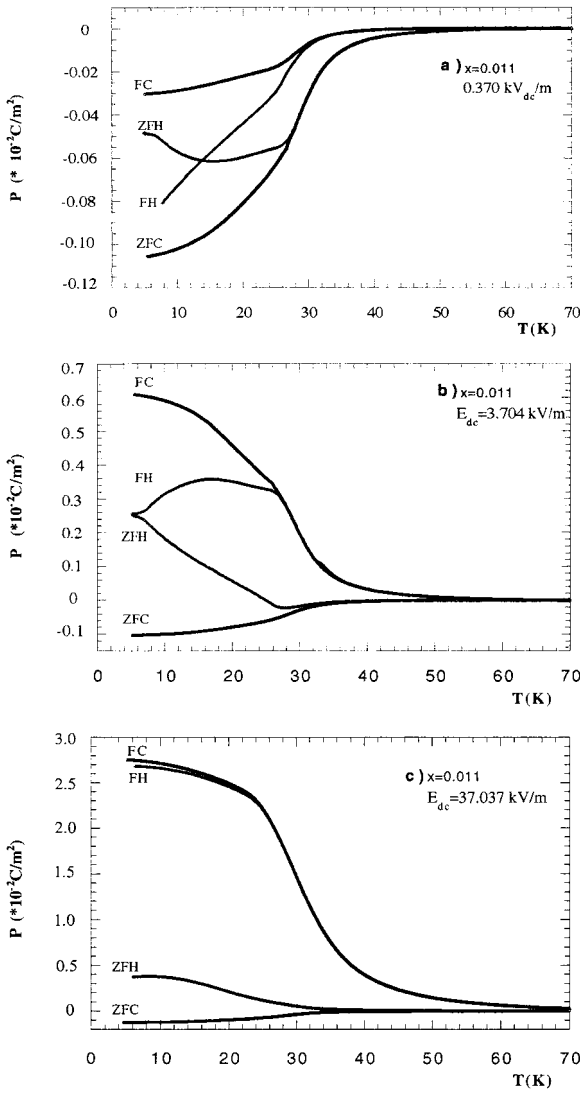

Figure 4. Examples of $P(T)$ curves measured in ZFC–FH–FC–ZFH cycles for $x = 0.011$: (a) $E = 0.370$ kV m^{-1}, (b) $E = 3.074$ kV m^{-1} and (c) $E = 37.037$ kV m^{-1}. As in $x = 0.005$ samples, the Almeida–Thouless temperature decreases as the bias increases. A residual polarization is also observed in the ZFC runs.

where

$$q = \langle s^\alpha s^\beta \rangle = \frac{1}{\sqrt{2\pi}} \int \mathrm{d}z\, \mathrm{e}^{-z^2/2} \tanh^2 \left(\frac{sH(z)}{k_B T} \right) \tag{2a}$$

$$r = \langle s^\alpha s^\beta s^\gamma s^\delta \rangle = \frac{1}{\sqrt{2\pi}} \int \mathrm{d}z\, \mathrm{e}^{-z^2/2} \tanh^4 \left(\frac{sH(z)}{k_B T} \right) \tag{2b}$$

$$H(z) = H + J_0 M + J_1 q^{1/2} z. \tag{2c}$$

In these equations $H(z)$ represents the local random field, H is the applied field and J_0 and J_1 are respectively the mean value and the width of the Gaussian distribution that describes the

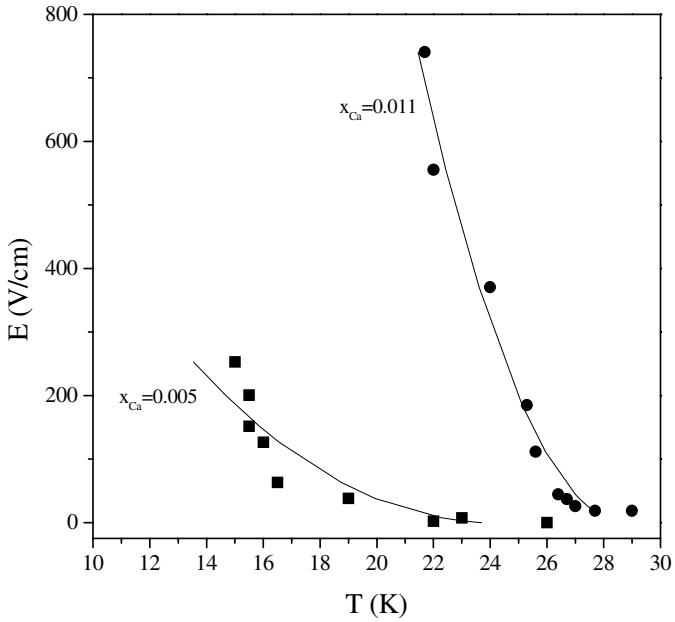

Figure 5. Electric field dependence of the ergodic to non-ergodic transition temperature (Almeida–Thouless temperature) for the compositions $x = 0.005$ (squares) and $x = 0.011$ (circles). The solid lines correspond to the best fits obtained by using the model discussed in the text.

random interactions J_{ij} between spins. The parameter q corresponds to the Edwards–Anderson parameter [30].

In principle, one could use the S–K equations (2*a–c*) to fit the experimental $E(T_{A-T})$ to equation (1). In PLZT ceramics, for example, the $E(T_{A-T})$ curve can be fitted to a power law $E = A[T(0) - T(E)]^{\gamma}$ with a exponent $\gamma \sim 1.5$ [31], as expected from the S–K equations (2*a–c*) in the limit of low applied fields and small Edwards–Anderson order parameter [20].

However, in strontium titanate, the destabilization of the ferroelectric order is phenomenologically described by assuming the existence of a lattice induced transverse field. The importance of this transverse field is reflected in the magnitude of the parameter T_1 in the Barrett formula [12]:

$$\varepsilon_1(T) = \frac{C}{(T_1/2)\coth(T_1/2T) - T_0} \tag{3}$$

that describes the temperature dependence of the dielectric constant in the paraelectric phase of SCT (T_1 range from about 36 K in pure ST [25] to 112 K in 1.1% Ca:SCT [22]).

The S–K equations (2*a–c*) have been modified to include the effect of an intrinsic transverse field and to generate the Barrett formula in the limit of high temperatures and low applied electric fields [16, 17]. The modified equations are:

$$q = \langle \eta^{\alpha}\eta^{\beta}\rangle = \frac{1}{\sqrt{2\pi}}\int \mathrm{d}z\, \mathrm{e}^{-z^2/2}\frac{\eta^2E^2(z)}{A^2+\eta^2E^2(z)}\tanh^2\left(\frac{\sqrt{A^2+\eta^2E^2(z)}}{k_BT}\right) \tag{4a}$$

$$r = \langle \eta^{\alpha}\eta^{\beta}\eta^{\gamma}\eta^{\delta}\rangle = \frac{1}{\sqrt{2\pi}}\int \mathrm{d}z\, \mathrm{e}^{-z^2/2}\frac{\eta^4E^4(z)}{(A^2+\eta^2E^2(z))^2}\tanh^4\left(\frac{\sqrt{A^2+\eta^2E^2(z)}}{k_BT}\right) \tag{4b}$$

$$E(z) = E + J_0P + J_1q^{1/2}z. \tag{4c}$$

In these equations $E(z)$ represents the local random field, P is the electric polarization, η the effective dipolar moment of a correlated domain and $2A = k_B T_1$ the transverse field energy.

The effect of a finite A can be tentatively included in equation (1) by considering the modified set of equations (4*a–c*) and by assuming $T(0)$ as an adjustable constant. Following this idea, we solved numerically this set of equations by using a self-consistent method and fitted the experimental $E(T_{A-T})$ curves to equation (1). The Levenberg–Marquardt nonlinear least squares fitting method was adopted in these fits. Note that, in this procedure, the S–K model corresponds to the particular case $A = 0$ and is therefore considered as a possible numerical solution.

The results of these numerical fits are depicted in figure 5 (solid lines). The values of the parameters adjusted to the experimental data are displayed in table 1.

Table 1. Values of the parameters obtained from the fitting of the $E(T_{A-T})$ data to the model discussed in the text.

	J_0/k_B (K)	J_1/k_B (K)	A/k_B (K)	η (e Å)	$T(0)$ (K)
$x = 0.005$	45.6	47.3	46.4	760	23.7
$x = 0.01$	80.7	81.4	80.8	153	28.7

As can be seen in figure 5, the experimental curves are roughly described by assuming a finite A. The quality of the fits is however different in the two compositions analysed. While the agreement between the fitted curve and the experimental points for $x = 0.011$ is good, the fit fails to describe an apparent change of regime observed in the experimental $E(T_{A-T})$ curve for $x = 0.005$. In fact, in the temperature range of 16 K $> T >$ 14 K, the $E(T_{A-T})$ curve for this latter composition seems to display a steeper variation that is not reproduced by the fit. Note that this lower temperature range corresponds to a close vicinity of the temperature $T^* = 12$ K where ε'' displays an anomaly that, being also observed in pure ST, cannot be directly related to the presence of calcium or to the calcium induced polar clusters. It seems therefore possible that the steeper variation observed in the $E(T_{A-T})$ in the lower temperature range may reflect the onset of a different mechanism not included in the model adopted.

Taking into account this limitation, one notes that the relative values of the parameters obtained in the fits ($J_1 > J_0 \sim A$) are, for the two compositions, consistent with the onset of a glass phase [17]. Moreover, if the value suggested in [16] for the dipolar moment per unit cell (0.2 e Å) is adopted, the values found for the average dipolar moment per cluster (η) would correspond to clusters of highly correlated dipoles involving 765 ($x = 0.01$) or 3800 ($x = 0.005$) unit cells. The clusters involved would correspond to polar ferroelectric nano-domains as suggested previously [32].

Finally, let us focus on the nature of the zfc polarization observed in all the compositions under study. If the zfc polarization were a spontaneous ferroelectric polarization it could be inverted by reversing the field. In this case, the field heating and the field cooling polarization curves obtained under fields of opposite signs should be symmetric with respect to the line $P = 0$. Therefore, during several thermal cycles, we investigated the effect of reversing the applied fields on the polarization curves.

Figure 6 illustrates typical curves obtained in these measurements on samples corresponding to $x = 0.005$ (figures 6(a) and (b)) and $x = 0.011$ (figures 6(c) and (d)). For the two compositions, the fh and fc polarization curves measured under opposite bias fields are quite different. Moreover, the zfh $P(T)$ curves obtained after heating and cooling at low fields display interesting features. In fact, if the previously applied bias field reinforces the zero-field polarization (figures 6(a) and 6(c)), the depolarization curve merges smoothly with the zfc curve, as expected for a thermally activated relaxation. However, if the previous bias

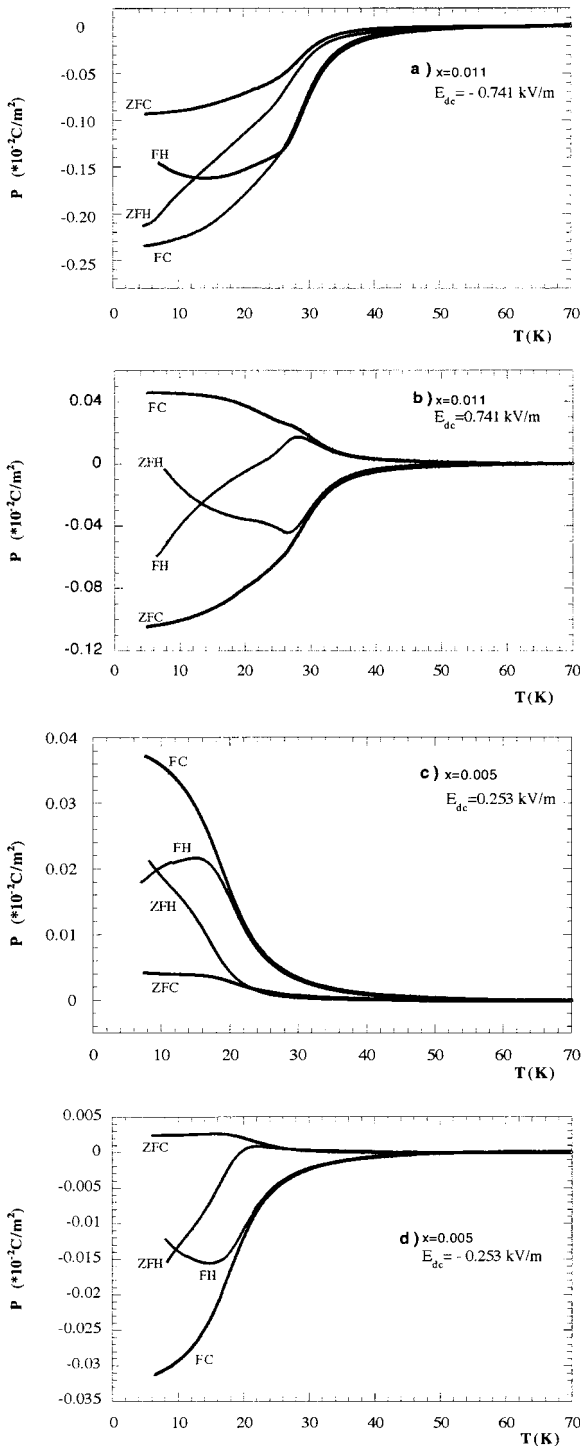

Figure 6. Examples of ZFC–FH–FC–ZFH polarization cycles measured under opposite bias fields plots for $x = 0.011$ ((a) $E = -0.741$ kV m^{-1} and (b) $E = 0.741$ kV m^{-1}) and for $x = 0.005$ ((c) $E = 0.253$ kV m^{-1} and (d) $E = -0.253$ kV m^{-1}).

field has a reversed sense with respect to the zfc polarization, the zfh curve displays a steeper variation and reverses its signal before a complete depolarization.

The asymmetry of the $P(T)$ curves measured under opposite external fields indicates that, for the field strengths tested, there is a component of the polarization that could not be inverted by the fields. Within the experimental error, this component corresponds roughly to the detected zfc polarization. This strongly suggests that this polarization may not be reoriented by an external field and may not correspond therefore to a spontaneous ferroelectric polarization. Its origin may be rather linked to the defect induced random fields that tend to stabilize a disordered domain state. In this sense, the zfc polarization may be seen as due to a remanent internal bias induced by the distribution of polar defects in the highly polarizable host lattice.

The strength and orientation of this internal bias may depend on the particular configuration of the defects, that act as nucleation centres of the polar nano-regions, as well as on the pattern of antiferroelastic domains stabilized below $T_{c1} \sim 105$ K. Thus, in principle, the internal bias could be dependent on kinetic parameters, such as the cooling rate adopted, as well as on external elastic or electrical fields.

As a preliminary step to check this latter possibility, we tried to see up to what extent the defect induced bias could be altered by an external electric field. We studied several cycles under opposite fields of increasing strength, in samples corresponding to $x = 0.005$ and $x = 0.011$. For the first composition, a threshold field of $E = 13$ kV m^{-1} was found, above which an external field applied in fc and fh runs could reverse the sign of the polarization observed in a subsequent zfc run. For $x = 0.011$, and in the range of field strengths tested (0–80 kV m^{-1}), the external voltage could not reverse the internal bias. Further studies are needed to fully elucidate the effect of external parameters in the behaviour of the zfc polarization and to shed more light on the microscopic mechanisms involved.

4. Conclusions

The results reported show that the inclusion of calcium in ST induces a weak non-ergodic regime at low temperatures. Previous studies on the time dependence of the dielectric constant suggest that this regime may reflect a true ergodicity breaking, in the sense that the equilibrium states reached after large times are dependent on initial conditions.

The analysis of the temperature dependence of the electric polarization in several thermal cycles under different bias fields allowed a determination of the Almeida–Thouless line that separates the ergodic and the non-ergodic regions in the T–E plane. The values of the Almeida–Thouless temperature at zero field $T_{A-T}(0)$ obtained are in very good agreement with the temperatures T_B below which the Barrett formula cannot describe the temperature dependence of ε' [22], which are $T_B \sim 25$ K for $x = 0.005$ ($T^{**} = 17$ K, $T(0) = 23$ K) and $T_B \sim 30$ K ($T^{**} = 27$ K, $T(0) = 29$ K) for $x = 0.01$.

A preliminary analysis of field dependence of the Almeida–Thouless temperatures, although purely heuristic and, at the present moment, not fully supported theoretically, stresses the importance of tunnelling in the dielectric behaviour of SCT. Moreover, the values of the parameters obtained from the fit of the A–T curve are consistent with a stabilization of a disordered polar phase, in which ferroelectric nano-domains are randomly frozen.

Acknowledgments

We thank gratefully Professor J G Bednorz for providing excellent single crystals. We are very much indebted to A Costa for his technical assistance in the dielectric and pyroelectric measurements. This work was partially supported by Projecto Praxis XXI/P/FIS/14287/98.

References

[1] Mueller K A and Burkard H 1979 *Phys. Rev.* B **19** 3593
[2] Shirane G and Yamada Y 1969 *Phys. Rev.* **117** 858
[3] Cowley R A 1962 *Phys. Rev. Lett.* **9** 159
[4] Viana R, Lunkenheimer P, Hemberger J, Boehmer R and Loidl A 1994 *Phys. Rev.* B **50** 601
[5] Vugmeister V E and Glinchuk M D 1990 *Rev. Mod. Phys.* **62** 993
[6] Bednorz J G and Mueller K A 1984 *Phys. Rev. Lett.* **52** 2289
[7] Mueller K A 1985 *Japan. J. Appl. Phys.* **24** (suppl. 24-2) 89
[8] Hoechli U T, Knorr K and Loidl A 1990 *Adv. Phys.* **62** 993
[9] Kleemann W 1993 *Int. J. Mod. Phys.* B **7** 2469
[10] Bianchi U, Dec J, Kleemann W and Bednorz 1995 *Phys. Rev.* B **51** 8737
[11] Maglione M, Lopes dos Santos M, Chaves M R and Almeida A 1994 *Phys. Status Solidi* b **181** 73
[12] Barrett J H 1952 *Phys. Rev.* **86** 118
[13] Dec J and Kleemann W 1998 *Solid State Commun.* **106** 665
Kleemann W, Dec J and Westwanski B 1998 *Phys. Rev.* B **58** 8985
[14] Blinc R and Zeks B 1974 *Soft Modes in Ferroelectrics and Antiferroelectrics* (Amsterdam: North-Holland)
Zhong W L, Zhang P L, Wang Y G and Qu B D 1997 *Ferroelectrics* **197** 15
Wang Y G, Kleemann W, Zhong W L and Zhang P L 1998 *Phys. Rev.* B **57** 13 343
[15] Sherrington D and Kirkpatrick S 1975 *Phys. Rev. Lett.* **35** 1972
[16] Ribeiro J L, Lacerda-Arôso M T, Chaves M R, Maglione M and Almeida A 1999 *J. Phys.: Condens. Matter* **11** 1247
[17] Almeida B G, Lacerda-Arôso T, Ribeiro J L, Chaves M R and Almeida A 2000 *Ferroelectrics* **239** 205
[18] Alberici F, Chaves M R, Doussineau P, Lacerda-Arôso T and Levelut A 1997 *J. Phys.: Condens. Matter* **9** 6447
[19] Bouchaud J-P 1992 *J. Physique* I **2** 1705
[20] de Almeida J R L and Thouless D J 1978 *J. Phys. A: Math. Gen.* **11** 983
[21] Müller K A, Berlinger W, Capizzi M and Gränicher H 1970 *Solid State Commun.* **8** 549
[22] Chaves M R, Almeida A, Maglione M and Ribeiro J L 1996 *Phys. Status Solidi* b **197** 232
[23] Viana R, Lunkenheimer P, Hemberger J, Böhmer R and Loidl A 1994 *Phys. Rev.* B **50** 601
[24] Müller K A, Berlinger W and Tosatti E 1991 *Z. Phys.* B **48** 227
[25] Hemberger J, Nicklas M, Viana R, Lukenheimer P, Loidl A and Boehmer R 1996 *J. Phys.: Condens. Matter* **8** 4673
[26] Bidaut O, Maglione M, Actis M, Kchikech M and Salce B 1995 *Phys. Rev.* B **52** 4191
[27] Chen A and Zhi Yu 2000 *Phys. Rev.* B **61** 11 363
[28] Dec J, Kleemann W and Westwanski B 1999 *J. Phys.: Condens. Matter* **11** L379
[29] Chen A, Zhi Yu, Lunkenheimer P, Hemberger J and Loidl A 1999 *Phys. Rev.* B **59** 6670
[30] Edwards S F and Anderson P W 1975 *J. Phys. F: Met. Phys.* **5** 965
[31] Viehland D, Li J F, Jang S J, Cross L E and Wuttig M 1992 *Phys. Rev.* B **46** 8013
[32] Bianchi U, Dec J, Kleemann W and Bednorz J G 1995 *Phys. Rev.* B **51** 8737